

## Mechanical analysis of a type of wire rope subjected to tension

Ma, Yuanxing; Shi, Baobin; Ali, Liaqat; Bai, Yong; Fang, Pan

**DOI**

[10.1080/17445302.2023.2190445](https://doi.org/10.1080/17445302.2023.2190445)

**Publication date**

2023

**Document Version**

Final published version

**Published in**

Ships and Offshore Structures

**Citation (APA)**

Ma, Y., Shi, B., Ali, L., Bai, Y., & Fang, P. (2023). Mechanical analysis of a type of wire rope subjected to tension. *Ships and Offshore Structures*, 19 (2024)(4), 541-547.  
<https://doi.org/10.1080/17445302.2023.2190445>

**Important note**

To cite this publication, please use the final published version (if applicable).  
Please check the document version above.

**Copyright**

Other than for strictly personal use, it is not permitted to download, forward or distribute the text or part of it, without the consent of the author(s) and/or copyright holder(s), unless the work is under an open content license such as Creative Commons.

**Takedown policy**

Please contact us and provide details if you believe this document breaches copyrights.  
We will remove access to the work immediately and investigate your claim.



## Mechanical analysis of a type of wire rope subjected to tension

Yuanxing Ma, Baobin Shi, Liaqat Ali, Yong Bai & Pan Fang

To cite this article: Yuanxing Ma, Baobin Shi, Liaqat Ali, Yong Bai & Pan Fang (2023): Mechanical analysis of a type of wire rope subjected to tension, Ships and Offshore Structures, DOI: 10.1080/17445302.2023.2190445

To link to this article: <https://doi.org/10.1080/17445302.2023.2190445>



Published online: 16 Mar 2023.



Submit your article to this journal [↗](#)



Article views: 26



View related articles [↗](#)



View Crossmark data [↗](#)



# Mechanical analysis of a type of wire rope subjected to tension

Yuanxing Ma<sup>a</sup>, Baobin Shi<sup>a</sup>, Liaqat Ali<sup>a</sup>, Yong Bai<sup>a</sup> and Pan Fang<sup>b</sup>

<sup>a</sup>College of Civil Engineering and Architecture, Zhejiang University, Hangzhou, People's Republic of China; <sup>b</sup>Department of Maritime and Transport Technology, Delft University of Technology, Delft, Netherlands

## ABSTRACT

Wire ropes are widely observed in many industries such as marine engineering and civil engineering, as a type of structure that can bear huge axial force. There are various kinds of wire ropes in practical engineering, corresponding to different usage scenarios. This paper focuses on  $6 \times 36\text{SW} + 1\text{WR}$  with a diameter of 16 mm. The axial mechanical properties of the wire rope are investigated by experimental, theoretical, and numerical methods. The stress–strain curve and ultimate strength of the steel wire rope obtained in the test are compared with the corresponding results from the finite element simulation. The comparison demonstrates the accuracy and reliability of the finite element model. In addition, a series of parametric studies are conducted to investigate the influence of pitch length and friction coefficient, etc. The purpose of this paper is to propose an accurate and efficient finite element model for the mechanical analysis of wire ropes.

## ARTICLE HISTORY

Received 9 September 2022  
Accepted 9 March 2023

## KEYWORDS

Wire Rope; tension; FEM;  
Parametric studies

## 1. Introduction

Steel wire rope is used in many projects, such as elevators, suspension bridges, ships, and ocean mooring engineering (Costello 1997; Feyrer 2015). The research shows that steel wire rope has a great ability to bear axial force and deformation with high stability. In addition, the steel wire rope is different from other structures, such as steel bars. The steel wire rope is composed of several elements. Generally, the core and strands are composed of multiple thin ropes, and then the strand rope is wound around the core (Figure 1), which provides the advantage of not breaking suddenly. Therefore, they can fulfil the task despite breaking one component or more. This is very important to ensure that the wire rope is tough and, in a sense, it is tolerable to take the form of broken wires or strands (Asmaa et al. 2014; Mouradi et al. 2018). The mechanical properties of ropes vary with different diameters, and tests are often conducted to compare (Utting and Jones 1985; Boroška et al. 2014; Jong 2015).

In the past decades, to characterise the mechanical behaviour of in-service steel wire rope, researchers have accurately simulated the complex geometric structure of spiral steel wire rope strands and ropes, developed geometric parameter equations, and further achieved geometric modelling, which can generate the geometry model of single-layer or multi-layer ropes and multi-strand ropes (Xiang et al. 2015; Orzłowska 2018). These existing geometric models fully consider the single helix structure of the single wire in the stranded strand and the double helix structure of the single wire in the wound strand. The mathematical expression of the single helix and double helix adopts the form of a parameter equation with variable input parameters to determine the centre lines of right or left strands and the centre lines of lang's or regular structures of any round steel wire rope. Researchers (Stanova et al. 2011a) derived the specific form of the parameter equation. Then by comparing the experimental data with the theoretical data, the three-dimensional geometric model of multi-layer strands and the finite element analysis results are verified. The obtained results confirm the correctness of the derived parameter equation and the importance of the established finite element model in mathematics and physics (Stanova et al. 2011b).

To monitor the evolution of wire rope damage and reliably determine the service conditions, an experimental study was conducted to track the evolution process of  $19 \times 7$  damage of non-rotating wire rope, and determine its different stages and the critical life fraction indicating the sudden failure of wire rope (Mouradi et al. 2018). The researchers established an analytical model to estimate the reliability and damage of steel wire rope from the reliability of steel wire rope components. In addition, the influence of friction effect on the mechanical behaviour of layered spiral structure wire rope (typical  $7 \times 7$ ) was conducted. The internal forces of ropes with friction, such as tension and torque, were compared with those without friction. The results show that the internal force of the rope with friction is generally more significant than that of the rope without friction (Gnanavel et al. 2010; Argatov 2011; Liu et al. 2019).

From the current research, most of the papers do not study  $6 \times 36\text{SW} + \text{IWR}$  wire rope by experiment, theory, and numerical simulation. In addition, most of the studies only considered parameters such as the surface wear of steel wire rope, yet many other factors were not considered. Therefore, based on the rich experience of experiment and finite element simulation, this paper conducts an investigation, theory, and numerical simulation for specific steel wire rope to obtain the axial mechanical properties. The stress–strain curve and ultimate strength of the steel wire rope obtained in the test are compared with the corresponding results of the finite element simulation. The comparison results prove the accuracy and reliability of the finite element model. Then a series of parametric studies were carried out to study the effects of pitch length, friction coefficient, and structure. Finally, an accurate and efficient finite element model is proposed for the mechanical analysis of steel wire rope.

## 2. Experiment

### 2.1. Dimensions and properties

The experimental samples are 16 mm diameter  $6 \times 36\text{SW} + \text{IWR}$  steel wire rope with a metallic core and crossed to the right (Figure 2). The helix structure of the wires and the strands is a vital

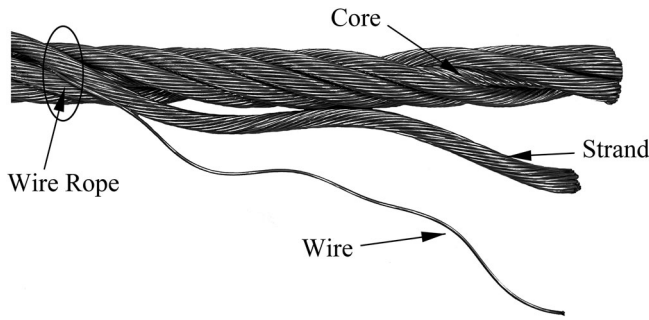


Figure 1. Components of wire rope.

characteristic of wire rope, as will be explained in detail later. The two main reasons this helix structure is used are an increase in bending flexibility and creating bundle coherence. This does, however come at the cost of axial strength and axial stiffness. With such a character, this rope is rugged and widely used in industry, mainly for lifting applications. It is spiral wound by 6 strands around a straight steel wire. The parameters were obtained with the uncoiling steel wire rope. The sample #1 is shown in Figure 3. The studied wire rope's main geometric and mechanical properties are shown in Table 1.

As mentioned earlier, our study aims to analyse the axial mechanical properties of 36SW + IWR wire rope. Therefore, the final five results are analysed and compared through the breaking tensile test of 5 steel wire ropes. The test samples are prepared with a length of 800 mm. The terminal connects a sample's end to the machine jaw to prevent sliding between the assembly lines or machine jaws. This operation also allows the specimen to be fixed so that the load is applied as axially as possible. WE-60 hydraulic universal material testing machine (Figure 4(a)) is used for static tensile test, and 2 mm/min of deformation corresponding to displacement is applied. The temperature is 20°C, and the humidity is 62%. The computer allows digital determination of the force and displacement during the experiment before fracturing. Figure 4(b) shows the assembly used for the tensile test. In addition, YYU-10/50 electronic extensometer (Figure 4(c)) is used to measure the sample, with a nominal accuracy of 0.001 mm. Four same positions are marked on five steel wire ropes. The diameter, lay angle, and lay length at each position are measured. The average value of each parameter is taken as the final result. Table 2 represents the final primary data.

## 2.2. Experiment results

Five steel wire ropes are tested. When the deformation reaches 5 mm, the extensometer is withdrawn. The yield load and breaking load of each steel wire rope are recorded. Before each steel wire rope is tested, the clamping position of the clamp is not exactly the same, so the gauge extension is different, and the error is controlled by 5%. The elastic modulus and elongation of each steel wire rope can be calculated by computer. The damage to each steel wire rope is also recorded. The steel wire ropes after the test are shown in Figure 5. Table 3 shows the corresponding test results of five steel wire ropes.



Figure 2. Right lay.



Figure 3. Experimental sample #1.

Table 1. Main features of the experimental rope.

Geometric and mechanical properties	Data
Diameter (mm)	D = 16mm
Construction	6 × 36SW + IWR
Nature and direction of the wiring	Ordinary lay on the right Right wiring in the inner layer Left wiring in the outer layer
Core nature	Metallic
The surface quality of the wires	Galvanized steel
Minimum breaking strength	189kN
Mass per unit length (kg/m)	1.004 kg/m
Young modulus of the wire (MPa)	E = 105,000MPa
Poisson's ratio	ν = 0.25

The section of each steel wire rope is calculated by weighing method, and the corresponding yield strength and tensile strength are calculated according to the stress formula. At the same time, the strain measured by the extensometer before deformation of 5 mm is calculated by formula (2.1), and the strain after deformation of 5 mm is calculated by formula (2.2). Finally, a curve is made according to the obtained stress strain.

$$\varepsilon = \frac{\Delta}{500} \quad (1)$$

$$\varepsilon = 1\% + \frac{u - u_{1\%}}{L_1} \quad (2)$$

Where  $\varepsilon$  is the strain,  $\Delta$  is the deformation determined by the extensometer,  $u$  is the deformation,  $u_{1\%}$  is the deformation when  $\Delta = 5$  mm, and  $L_1$  is the Gauge elongation. All Stress–Strain curves are obtained through the following process:

- (1) Sorting out the recording data of 5 ropes in the experiment, including load, deformation, and deformation determined by extensometer.
- (2) Using formulas 2.1 and 2.2 to calculate the strain.

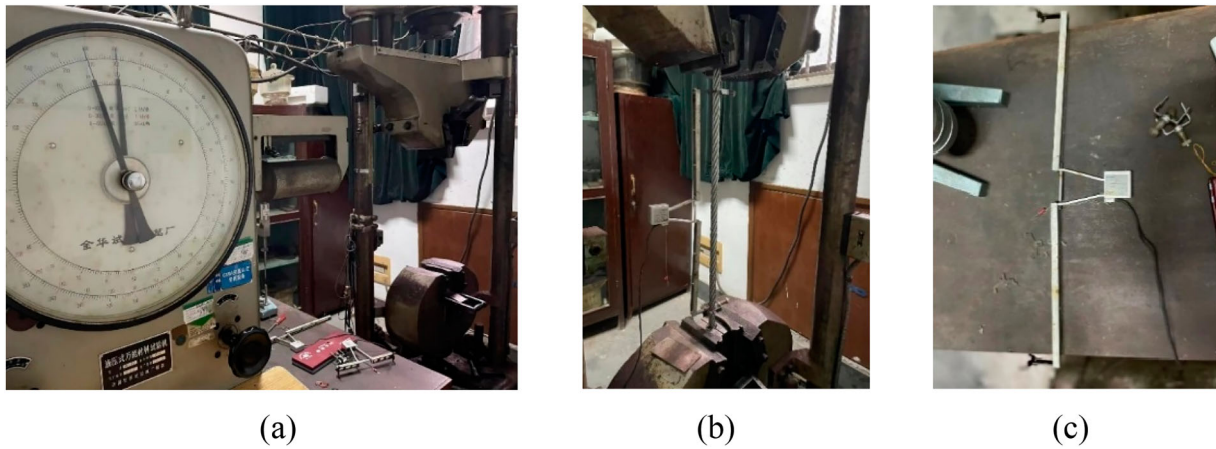


Figure 4. (a) Experimental machine. (b) Tensile experiment. (c) Electronic extensometer.

Table 2. Basic information of ropes.

Sample	Diameter (mm)	Total length (mm)	Valid length (mm)	Lay angle (°)	Lay length (mm)
#1	15.9	800	600	73	111
#2	16.4	801	602	71	110
#3	16.6	797	600	71	111
#4	16.5	803	596	72	111
#5	16.6	798	599	73	111

- (3) Obtaining the stress at different strains with the equation:  $\sigma = P/A$ , in which  $\sigma$  refers to stress,  $P$  refers to load, and  $A$  refers to the cross-sectional area of the rope. According to the actual diameter determination of core and wire,  $A$  is calculated out  $106.37\text{mm}^2$ ,  $104.06\text{mm}^2$ ,  $105.24\text{mm}^2$  when lay angle equals to  $17^\circ$ ,  $19^\circ$ ,  $18^\circ$  respectively.
- (4) All samples have almost 300–400 data points, with the premise that ignoring useless points. The stress–strain curve can be drawn using these points, which are enough to ensure accuracy.

It is true that the stress is not zero under the condition of no strain, and this phenomenon does not conform to the mechanical laws. After investigating, the reason why this happened is that

there existed a low load before the experiment started. Therefore, to eliminate the error, data points which include the deformation less than 0.1 mm are filtered out. Stress–strain curves are plotted in a graph, see Figure 6.

It can be seen that there exists an inflexion point when strain reaches 1%, which reflects that a total different formula is used to calculate strain as deformation exceeds 5 mm. Also It can be found that 5 ropes have similar maximum stress after the ultimate strain occurs. Different shapes and colours represent different ropes and an average curve after fitting is drawn in order to make comparison with 5 curves of 5 ropes and a curve obtained from simulation.

### 3. Theoretical analysis

#### 3.1. Basic assumption

The theory of this paper is based on the assumption that each wire is represented as a supported beam, and the entire section is described as an independent beam (Jong 2015).

- (1) Each wire behaves as a Euler-Bernoulli beam. This is the basis of the thin rod model.

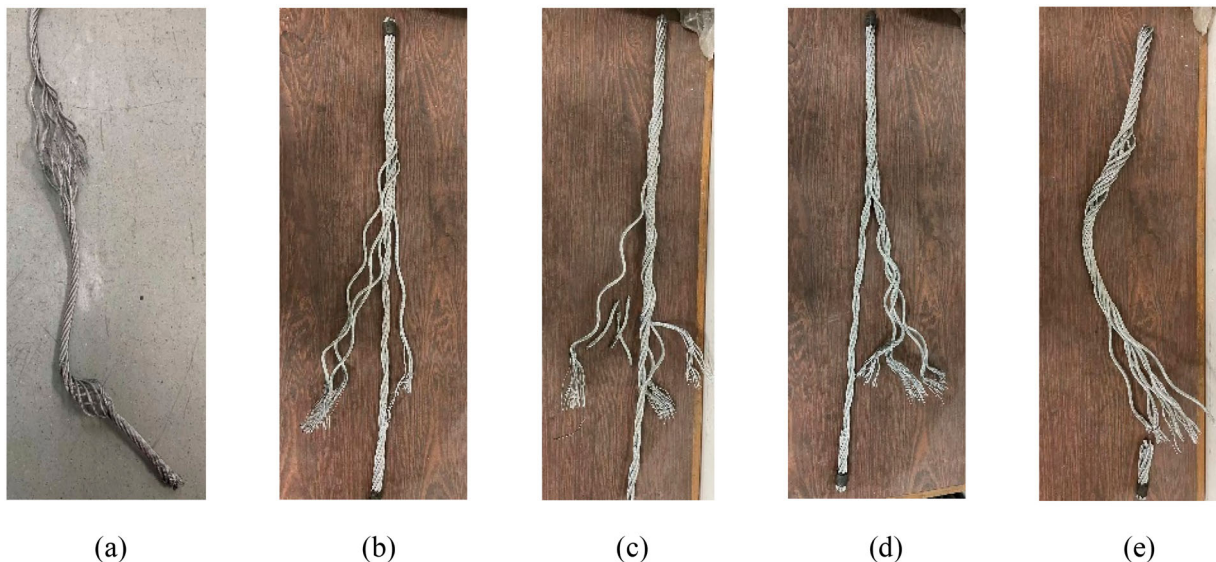
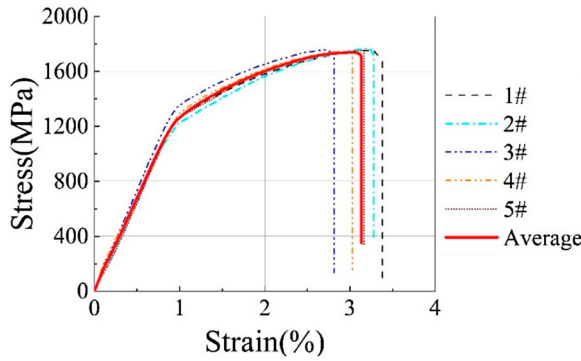


Figure 5. Damage condition of 5 samples: (a)~(e) respectively sample#1~#5.

**Table 3.** Test results.

Sample	Yield strength (kN)	Tensile strength (kN)	Gauge elongation (mm)	Elastic module (10 <sup>5</sup> MPa)	Damage condition
#1	142.1	186.6	623	1.075	Intermediate failure
#2	133.0	184.0	602	1.075	Upper-end failure
#3	147.5	182.8	600	1.135	Lower end failure
#4	146.6	183.7	590	1.015	Lower end failure
#5	140.2	184.3	595	1.110	Lower end failure

**Figure 6.** Stress-strain curve of 5 wire ropes.

- (2) The behaviour of the material is bilinear with some plastic deformation. Plastic deformation needs to be considered to simulate the failure of metal wires.
- (3) There is no contact between wires in the same layer.
- (4) Ignore the ellipse of the rope.
- (5) According to Feyrer theory (Feyrer 2015), the change of laying angle has little effect on bending stress.
- (6) According to (Papailiou 1995), the friction behaviour is bilinear.
- (7) No friction after reaching the transitional curvature.
- (8) Elastoplastic constitutive model is adopted, using fracture failure defined by the flexible damage model

#### 4.1. Calculation formula

When a steel wire rope is tensioned for the first time, all the steel wire ropes are slightly sunken, and the steel wire rope bears a large extension with a deficient force. This highly nonlinear effect is usually eliminated by applying pressure to the rope before actual use. Once the rope sinks and tightens again, the central line will bear the maximum tension. The single line and double helix will expand less than the centre line because they are at an angle with the centre of mass, so there will be lower stress than the centre wire rope. This means the central wire is the first to yield and the last to fail in the axially loaded wire rope. The axial stress of straight-strand steel wire can be calculated according to formula 3.1.

$$\sigma_t = \frac{\cos^2 \alpha_k E_k}{\sum_i \cos^3 \alpha_i E_i A_i} F \quad (3)$$

For the whole wire rope, the expression is extended to formula 3.2.

$$\sigma_t = \frac{\cos^2 \alpha_k E_k}{\sum_i (\cos^3 \alpha_i) \sum_{ij} (\cos^3 \alpha_{ij}) E_{ij} A_{ij}} F \quad (4)$$

$\sigma_t$  is the stress in a wire parallel to the wire,  $\alpha$  is the lay angle of the wire or strand respectively,  $F$  is the external axial force,  $E$  is the modulus of elasticity, and  $A$  is the cross-sectional area of a wire; Subscript  $k$  refers to a specific wire, subscript  $l$  refers to a specific strand, subscript  $i$  refers to all wires in a layer, subscript  $j$  refers to all strands in a wire rope.

A table is listed including all calculated stress of 5 ropes by using two theoretical formulas, with breaking tensile load 189kN (see Table 4).

It can be found that the maximum calculated tensile stress occurs in the centre wire of core and the minimum calculated tensile stress occurs in the strand wire of strands. Also the phenomenon that the stress in the strand wire of core equals to the stress in the centre wire of strands suits to the theory in this article. Moreover, with increasing lay angle, the stress has bigger maximum tensile stress, which draws forth the parametric study on lay angle.

For the wire rope with Poisson's coefficient of 0.3, the lateral shrinkage has little effect on the internal stress of the wire rope. The pressure difference is 2% to 3%. For other materials, such as fibre rope core, it can lead to more significant differences.

#### 5. Finite element simulation

The finite element simulation of wire rope is very complex, especially for multi-strand wire rope. The model in this paper is directly established in ABAQUS, with a length of 150 mm and a lay length of 110 mm. This paper assumes that the elastic modulus of metal wire material is  $E = 105,000$  MPa and the density is  $\rho = 5000$  kg/m<sup>3</sup>, Poisson's ratio  $\nu = 0.25$ . The wire is made of uniform, isotropic and linear elastic material. Only the elastic region of multi-layer chain behaviour is considered. The finite element type is designated as solids. Each node has 3 degrees of freedom. To reduce integration, the mesh generation is controlled by an hourglass. Hourglass mode is a non-physical zero energy deformation mode that generates zero strain and stress. The mesh for each line is generated independently. The element type used for modelling is C3D8R, a hexahedral reduced integral element of 8 nodes. For reduced integral element, it needs to be divided into fine grids to overcome the hourglass problem. Allowing for the calculating accuracy and efficiency of solution, the grid size of this model is determined as 1mm, and the local picture of grid in detail is taken as Figure 7.

The type of surface-to-surface contact is defined as between the surfaces of a single adjacent wire. The general contact algorithm in ABAQUS/explicit is used for contact, and the contact pair is automatically generated. The created normal behaviour contact attribute is hard to contact, and penetration behaviour is not allowed between contact pairs. The tangent behaviour contact attribute is

**Table 4.** Calculated maximum tensile stress of 5 ropes.

Sample	Tensile strength (kN)	Lay angle (°)	Core (MPa)		Strands (MPa)	
			Centre wire	Strand wire	Centre wire	Strand wire
#1	186.6	17	1912.59	1829.02	1371.77	1311.83
#2	184.0	19	1970.43	1863.08	1397.31	1321.19
#3	182.8	19	1957.58	1850.93	1388.2	1312.72
#4	183.7	18	1923.34	1829.2	1371.9	1304.75
#5	184.3	17	1889.02	1806.48	1354.86	1295.66

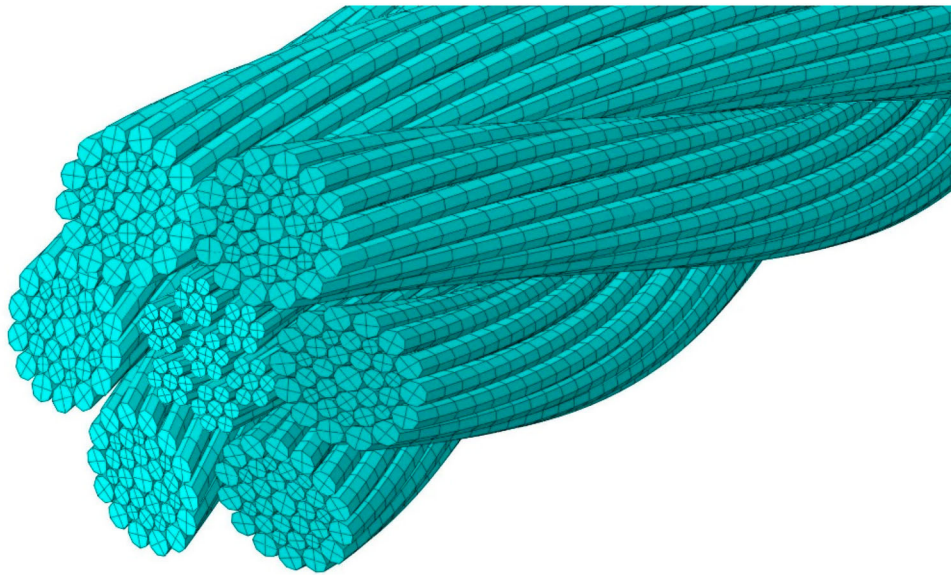


Figure 7. Grid model.

friction contact based on the penalty friction formula, and the friction coefficient is a fixed value set to 0.2.

Set the sections at both ends of the wire rope as a set, and concentrate them at the centre point to set constraints (Figure 8(a)). All numerical analyses of the axial behaviour of the chain are carried out with one end clamped (displacement disabled) and the other end applied with a force (longitudinal axial displacement). Axial force can be used to both ends of the cable, preventing rotation or rotating freely. Because the laboratory test is carried out under the condition of a fixed end, the axial rotation of the end of the steel strand is restrained in the numerical study. Shrinkage of the steel wire section (and strand section) is considered. According to the given boundary conditions, the nodes' degrees of freedom at both ends of the steel strand finite element model are determined. The boundary conditions of clamped end strands are shown in Figure 8(b). Then, apply a load with a displacement of 20 mm to the end whose displacement is not limited.

Through simulation, it can be observed that the wire rope breaks at the upper part of the middle part (Figure 9(a)), which is very

close to the actual failure situation. Also, the distribution of the tensile stress of the rope is corresponding to the theory.

## 6. Comparison and discussion

In the beginning, the rope has a process of tension, which creates some unnecessary data points for simulation. The material model of wire rope simulates the damage characteristics of materials after entering the plastic stage through the ductile damage model. After considering the damage effect, the strength and stiffness of the damaged part of the material both show a downward trend until failure, which can simulate the process of tensile fracture of steel wire.

Therefore, the state when the rope starts to stretch elastically is regarded as the initial state, and the data points before this initial state are all omitted. The stress-strain curve comparison between the test and the finite element steel wire rope (Figure 10) can be obtained. It can be seen that two curves fitted well, with the error about 4%.

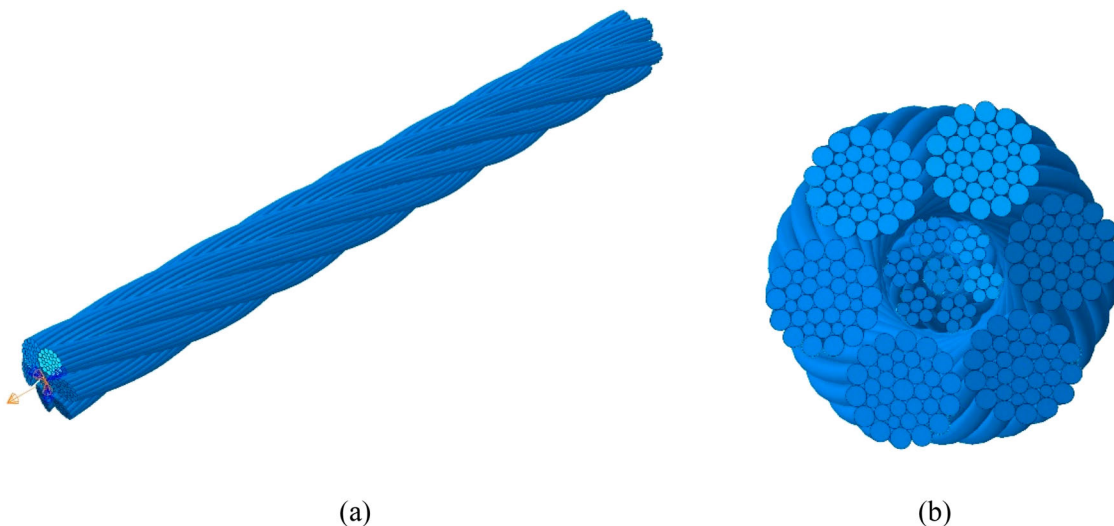


Figure 8. (a) Boundary conditions of clamped end strands. (b) Cross-section of rope.

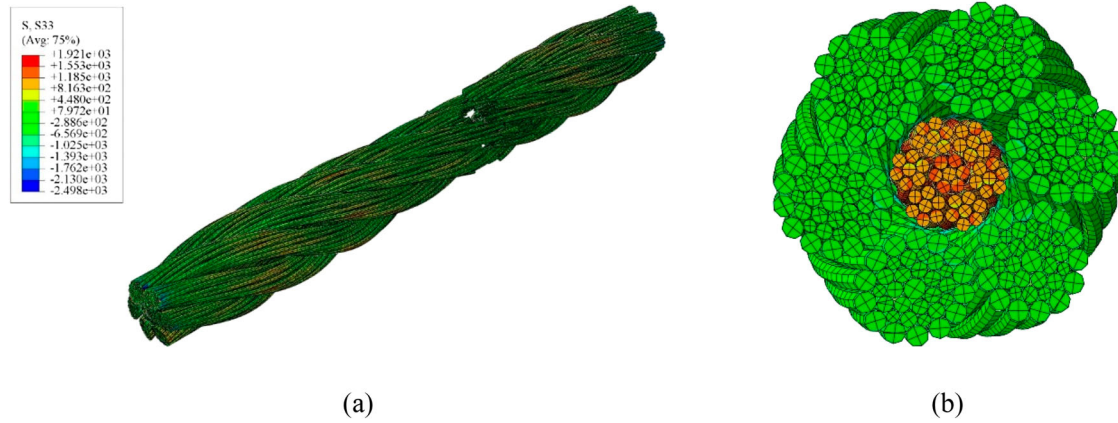


Figure 9. (a) Distribution of the tensile stress of the rope and breaking. (b) Distribution of tensile stress of the rope in cross-section.

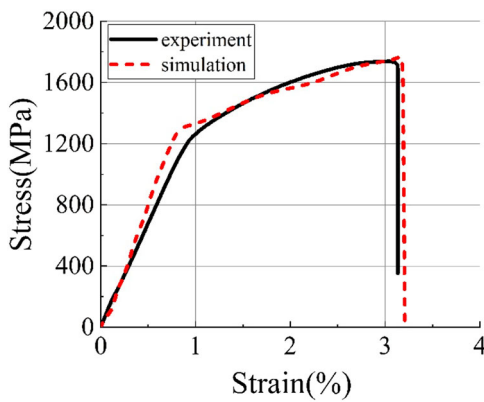


Figure 10. Comparison between experiment and FEM.

When testing the straight wire rope, it was found that the breaking load was slightly higher than the MBL given by the manufacturer. This seems reasonable because the manufacturer may include some additional safety measures to ensure that accidents do not occur. Not all wire ropes fail at the socket. The resin connection between the wire rope and the socket is stronger than the wire rope itself. At about 90% of the breaking load, the sound of wire breaking can be heard. No wire is broken, indicating that the wire inside the wire rope is broken. This matches with the general steel wire rope theory. The wire with a single helix or smaller helix angle is the first to break. Once the core fails, the rest of the wire rope will fail almost instantaneously. Redistribution between wires of outer strands is not possible. This is consistent with the small plastic deformation capacity of the material.

Table 5. Comparison of different lay length and friction coefficient.

Lay length	Friction coefficient	Yield strength (kN)	Tensile strength (kN)
70	0.2	100.0	140.6
90		114.6	168.5
110		141.2	189.7
130		144.6	199.0
150		140.8	210.9
110	0.1	141.2	186.6
	0.15	141.2	188.5
	0.2	141.2	189.7
	0.25	141.2	190.5
	0.3	141.2	191.0

## 7. Parametric studies

Many parameters affect the mechanical properties of steel wire rope. It is of great engineering significance to study the parameters of steel wire rope. It can observe the changes of mechanical properties under different parameters and consider the cost, service life, and other factors to optimise the design. The effects of various parameters (pitch length and friction coefficient) on the tensile mechanical properties of steel wire rope are analysed by FEM.

### 7.1. Pitch length

With the increase of lay distance, the breaking force of steel wire rope is increasing as a whole; When the lay distance is less than 90 mm, the breaking force of steel wire rope increases greatly, and the fluctuation range is large; When the lay distance is 90–130 mm, the breaking force of steel wire rope increases slightly, and the fluctuation range is small; When the lay distance exceeds 130 mm, the breaking force of the steel wire rope tends to increase, and the fluctuation range is large. The larger the lay distance, the greater the breaking force, and the larger the fluctuation range of the breaking force, which indicates that the mechanical property stability of the steel wire rope is poor. This is because the strength loss during the deformation of the steel wire during the twisting process is slight, and the corresponding breaking force is more prominent, but the looseness and fatigue resistance of the steel wire rope will be poor. The larger the lay distance, the smaller the twist deformation of the single wire in the twisting process of the steel wire rope, and the greater the elastic resilience. If this elastic resilience is not eliminated, the fatigue resistance of the steel wire rope will be reduced, and the service life will be shortened. Therefore, the lay distance should not be too large.

The lay distance greatly influences the comprehensive properties of the steel wire rope, and the mechanical properties play a significant role in the stability of the overall structure of the steel wire rope. The lay distance should not be too large or too small. A suitable small lay distance can reduce the bending stress of steel wire rope during fatigue tests and meet the requirements of mechanical properties.

### 7.2. Friction coefficient

In axially loaded ropes, the effect of friction is considered to be minor, especially when the outer cable is not in contact. In this case, the cross-section of the strand can be rotated about an axis passing through the centreline of the cable. In the case of a rope with a fibre core, the section cannot rotate freely about an axis passing

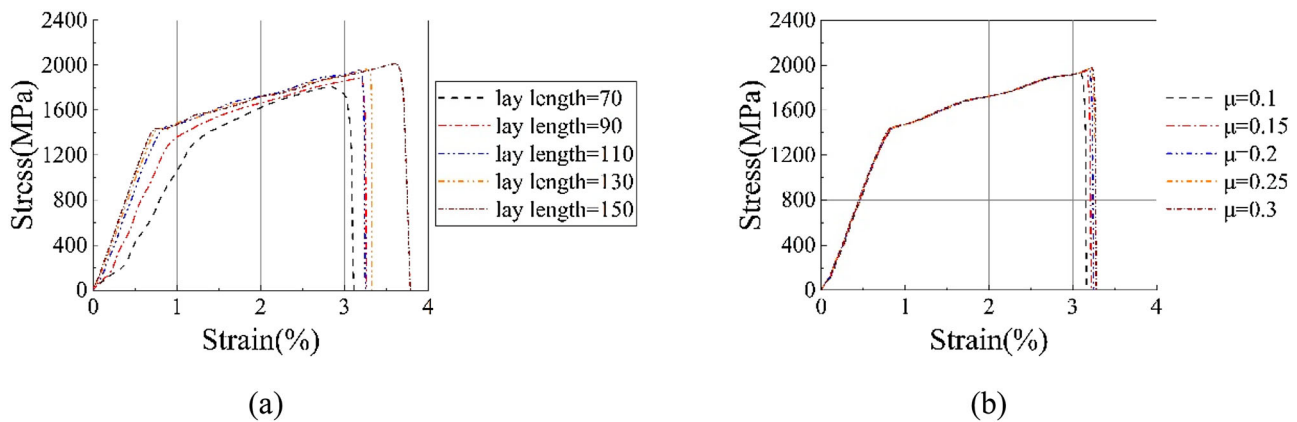


Figure 11. Stress–strain curves of different parameters: (a) lay length.(b) friction coefficient.

through the centreline of the rope, so friction has some effect. In the process of bending and stretching of steel wire rope with independent steel wire rope core, similarly, since the steel wire rope core tends to prevent the contact between strands, the outer strand tends to only contact with independent steel wire rope, and its behaviour is a bit like a simple strand. It can be observed that the change in friction coefficient has little influence on breaking tensile force.

The total load due to bending is considered to be small compared to the case of axial loading. The maximum force generated by friction is related to the axial force in the steel wire rope. As the spiral structure stretches, it grabs the lower layers and creates forces in the radial direction between them. A more clear comparison is demonstrated in Table 5 and Figure 11, which demonstrates the data support.

## 8. Conclusions

In this paper, the mechanical behaviour of steel wire rope under tension is studied by experiment, theory, and finite element method. The prototype test with five samples has been verified by analysis and finite element method. The theoretical approach is used to calculate to understand the mechanical properties of the rope as a whole. The above three methods are mutually verified and have good accuracy and reliability.

The lay distance greatly influences the comprehensive properties of the steel wire rope, and the mechanical properties play a vital role in the stability of the overall structure of the steel wire rope. The lay distance should not be too large or too small. A suitable small lay distance can reduce the bending stress of steel wire rope during fatigue tests and meet the requirements of mechanical properties.

In axially loaded ropes, the effect of friction is considered to be minor, especially when the outer cable is not in contact. In this case, the cross-section of the strand can be rotated about an axis passing through the centreline of the cable. In the case of a rope with a fibre core, the section cannot rotate freely about an axis passing through the centreline of the rope, so friction has some effect.

Based on the study of rich experience of experiment and finite element simulation, this paper carries out an experiment, theory and numerical simulation for specific steel wire rope to obtain the axial mechanical properties. The stress–strain curve and ultimate strength of the steel wire rope obtained in the test are compared with the corresponding results of the finite element simulation. The comparison results prove the accuracy and reliability of the finite element model. Then a series of parametric studies were carried out to study the effects of pitch length, friction coefficient, and structure. Finally, an accurate and efficient finite element model is proposed for the mechanical analysis of steel wire rope.

## Acknowledgements

The author thanks the analysis and testing centre of the school of Aeronautics and Astronautics of Zhejiang University for its help in using all necessary equipment for experimental research.

## Disclosure statement

No potential conflict of interest was reported by the author(s).

## References

- Argatov I. 2011. Response of a wire rope strand to axial and torsional loads: Asymptotic modeling of the effect of interwire contact deformations. *Int J Solids Struct.* 48(10):1413–1423. doi:10.1016/j.ijsolstr.2011.01.021.
- Asmaa C, Mohamed EG, Abdelkader B, Mostapha BE, Abdelilah H, Khalid EH. 2014. Analytical modeling and experimental characterization of residual resistance loss of broken wire ropes lifting. *Rev Energy Technol Policy Res.* 1(2):42–49. doi:10.18488/journal.77/2014.1.2/77.2.42.49.
- Boroška J, Pauliková A, Ivančo V. 2014. Determination of elastic modulus of steel wire ropes for computer simulation. *Appl Mech Mater.* 683:22–27. doi:10.4028/www.scientific.net/AMM.683.22.
- Costello GA. 1997. *Theory of wire rope.* Springer Science & Business Media.
- Feyrer K. 2015. *Wire ropes: tension, endurance, reliability.* Berlin: Springer Berlin Heidelbergdoi:10.1007/978-3-642-54996-0.
- Gnanavel BK, Gopinath D, Parthasarathy NS. 2010. Effect of friction on coupled contact in a twisted wire cable. *J Appl Mech.* 77(2):024501. doi:10.1115/1.3197141.
- Jong DCB. 2015. Analytical and experimental analysis of the capacity of steel wire ropes subjected to forced bending.
- Liu D, Zheng S, He Y. 2019. Effect of friction on the mechanical behavior of wire rope with hierarchical helical structures. *Math Mech Solids.* 24(7):2154–2180. doi:10.1177/1081286518816519.
- Mouradi H, El Barkany A, El Biyaali A. 2018. Steel wire ropes failure analysis: Experimental study. *Eng Fail Anal.* 91:234–242. doi:10.1016/j.engfailanal.2018.04.019.
- Orzłowska R. 2018. Experimental study of mechanical properties of steel cables. In: Urbańska-Galewska E, editor. *Matec Web conf.* 219. p. 002004. doi:10.1051/mateconf/201821902004.
- Papailiou KO. 1995. Bending of helically twisted cables under variable bending stiffness due to internal friction, tensile force and cable curvature.
- Stanova E, Fedorko G, Fabian M, Kmet S. 2011a. Computer modelling of wire strands and ropes Part I: Theory and computer implementation. *Adv Eng Softw.* 42(6):305–315. doi:10.1016/j.advengsoft.2011.02.008.
- Stanova E, Fedorko G, Fabian M, Kmet S. 2011b. Computer modelling of wire strands and ropes part II: Finite element-based applications. *Adv Eng Softw.* 42(6):322–331. doi:10.1016/j.advengsoft.2011.02.010.
- Utting WS, Jones N. 1985. Tensile testing of a wire rope strand. *J Strain Anal Eng Design.* 20(3):151–164. doi:10.1243/03093247V203151.
- Xiang L, Wang HY, Chen Y, Guan YJ, Wang YL, Dai LH. 2015. Modeling of multi-strand wire ropes subjected to axial tension and torsion loads. *Int J Solids Struct.* 58:233–246. doi:10.1016/j.ijsolstr.2015.01.007.